THE JOURNAL OF PHYSICAL CHEMISTRY C

Article

pubs.acs.org/JPCC

Unification of Two Different Melting Mechanisms of Nanovoids

Siqi Li[†] and Weihong Qi*[,†,‡,§]

[†]School of Materials Science and Engineering, Central South University, Changsha, 410083, P. R. China

[‡]Institute for Materials Microstructure, Central South University, Changsha 410083, P. R. China

[§]Key Laboratory of Non-ferrous Materials Science and Engineering, Ministry of Education, Changsha 410083, P. R. China

ABSTRACT: Void melting in solids is a very complicated process, while the mechanism is far from understood. In this paper, we studied the void melting in Pd and Si solids using a molecular dynamics simulation method. It is found that there exist two different melting mechanisms for nanovoid, nucleation melting and non-nucleation melting; although void melting in Pd follows the former mechanism, that in Si follows the latter (unless the nanovoid size decreases to a critically small value). For nucleation melting, there will be liquid nucleate at the surface of the nanovoid, and then the liquid fills the void before the temperature reaches the melting point of the solids. For non-nucleation melting, there will be local stiffening around the nanovoid, and the nanovoid always exists until the whole matrix comes to melt. For these two different melting mechanisms, the inner surface atoms will behave totally differently. We find the most exciting thing to be that the two mechanisms can be well unified based on surface melting theory. Furthermore, it is predicted that when the nanovoid decreases to a critical value the matrix solid may be superheated, which agrees well with the simulation of void melting in Pd and Si solid.

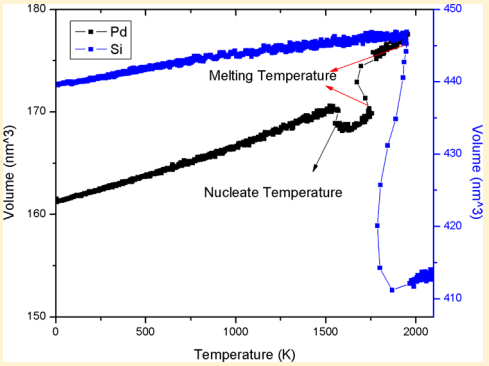

1. INTRODUCTION

Melting is a very common phenomenon in nature, and solid melting is a very complex process. Due to the fact that the mechanism for melting is far from understood, many researchers have paid their attention to investigating the melting of solids, especially in new structural materials. Due to special properties of solids[1,2] with voids at the nanoscale, a lot of literature reported the stability of voids, especially melting.[3−5] However, the melting of voids is also far from understood, which is also different from the melting of nanoparticles.[6−8] As for nanoparticles, in general, with decreasing particle size, their melting temperature may decrease for the free-standing surface[9−11] or increase for particles embedded in the matrix.[12−14]

There are two different melting mechanisms for void melting. One is the nucleation melting (NM) mechanism, which means the void melts first and then the whole void melts. The other is the non-nucleation melting (NNM) mechanism, where the void skin stiffens first and then the total crystal melts with increase of temperature and, meanwhile, the void disappears. For the NM mechanism, Li et al.[4] have studied the mechanism of the melting of nanovoids in the Ar matrix using molecular dynamics simulation (MD), and they found that the solid−vapor void surface is stable at a low temperature. With increasing temperature, a thin liquid layer nucleates around the void surface and grows until the liquid atoms fill the void completely, the liquid droplet stops growing, and the radius does not change even after very long MD steps. Last, the whole sample melts completely. He et al.[15] have studied the shock melting of single-crystal copper with a nanovoid, showing that under shock strengths heterogeneous local melting in the void-collapsed region occurs prior to homogeneous melting of the bulk material due to the high temperature of the hot spot effect as well as the low-energy barrier upon melting of the highly disordered collapsed region. Agrawal et al.[2] show that the void melting depends on void size, almost independent of void shape. Lu[16] and Li[17] have established thermodynamic models to explain the melting of nanovoids considering the surface energy. According to their theories, the surface energy of nanovoids increases with a decrease of size and finally reaches a plateau at a critical nanovoid size.

For the NNM mechanism, Ouyang et al.[18−20] think that the size-dependent surface or interface energy of nanovoids (which is a strong function of the lattice strain) plays a crucial role for the melting behavior when considering the negative curvature of the void. They proposed a physical picture for void melting: during heating, the nanovoid in the matrix first shrinks; meanwhile, its skin stiffens, and then the matrix melts first. At last, the nanovoid vanishes when the temperature increases further. Zhu et al.[1,21−24] have studied the nanovoids in the Si matrix using ion irradiation and electron beam irradiation. They found that the void first shrinks and always exists during local matrix melting, which is the experimental proof of the NNM mechanism.

There is no theory to explain why there exists a NM mechanism in some materials but NNM mechanism in others. To give a clear explanation on void melting, in this work, we studied void melting in Pd and Si solids using the MD method and found that void melting in Pd follows the NM melting mechanism and in Si follows the NNM mechanism (unless the nanovoid size decreases to a critical small value). The most

Received: November 24, 2014
Revised: February 3, 2015
Published: February 25, 2015

DOI: 10.1021/jp5117245
J. Phys. Chem. C 2015, 119, 6843−6851

exciting thing we found is that the two mechanisms can be unified based on surface melting theory.[17,25] This paper is organized as follows: section 2 gives the details of simulation;[26] section 3 shows the results of void melting in Pd and Si (the two refers to two different melting mechanisms, respectively); section 4 gives the thermodynamics considering void melting, which unifies the two mechanisms; and the conclusions are made in section 5.

2. SIMULATION DETAILS

The embedded atom method (EAM) has been widely used in the literature to predict the properties of metals alloys,[27,28] such as the surface energy and elastic constants of Pd accurately. It is adopted for simulating the melting of Pd presently. The total energy (E_{tot}) in the EAM is given by

$$E_{tot} = \sum_i F_i(\rho_{h,j}) + \frac{1}{2}\sum_{j\neq i} \varnothing_{ij}(R_{ij}) \quad (1)$$

where $F_i(\rho)$ is the embedding energy of atom i; $\rho_{h,j}$ is the host electron density at atom j due to the surrounding atoms; $\varnothing_{ij}(R_{ij})$ is a short-range electrostatic interaction between atom i and j; R_{ij} is the core distance between i and j atoms; and the sums are over all atoms.

The host electron density is approximated by the superposition of atomic densities

$$\rho_{h,j} = \sum_{j\neq i} \rho_j^a(R_{ij}) \quad (2)$$

where ρ_j^a is the atomic electron density, and approximately $\rho_j^a(R) = n_s\rho_s(R) + n_d\rho_d(R)$ (n_s and n_d are the number of outer s and d electrons, respectively, and ρ_x and ρ_d are the corresponding electron densities).

$\varnothing_{ij}(R)$ is given by the geometric mean of the individual effective charges Z

$$\varnothing_{ij}(R) = \frac{Z_i(R)Z_j(R)}{R} \quad (3)$$

where $Z(R) = Z_0(1 + \beta R^\nu)e^{-\alpha R}$, and Z_0 is assumed to be the number of outer electrons of the atom. Z_0, α, β, and ν are the four adjustable parameters used to fit the functions. The values for Pd are[27] $Z_0 = 10.0$, $\alpha = 1.4483$, $\beta = 0.285$, $\nu = 1$, and $n_s = 0.8456$.

The interactions between Si atoms are covalent bonds, thus we used the Stilllinger–Weber (SW) potential[29,30] (developed for Si and Ge) to compute the interactions between Si atoms. Thijsse[31] suggested that in fact the Stillinger–Weber potential is a special case of the modified embedded-atom method (MEAM) potential. SW potentials contain only pair and triplet terms in the forms

$$v_2(r) = \begin{cases} A(Br^{-p} - r^{-q})\exp[(r-a)^{-1}], & r < a \\ 0, & r \geq a \end{cases} \quad (4)$$

and

$$v_3(r_{ij}, r_{ik}, \theta_{jik}) = h(r_{ij}, r_{ik}, \theta_{jik}) + h(r_{ji}, r_{jk}, \theta_{jik}) + h(r_{ki}, r_{kj}, \theta_{jik}) \quad (5)$$

where A, B, p, and a are positive parameters, and θ_{jik} is the angle subtended between j and k at vertex i for any triplet of atoms. The function h is given by

$$h(r_{ij}, r_{ik}, \theta_{jik}) = \lambda \exp[\gamma(r_{ij} - a)^{-1} + \gamma(r_{ik} - a)^{-1}] \times \left(\cos\theta_{jik} + \frac{1}{3}\right)^2 \quad (6)$$

This function vanishes when $r_{ij} \geq a$ and $r_{ik} \geq a$. The values of the nine parameters in this work are[29] $A = 7.049556227$, $B = 0.6022245584$, $p = 4$, $q = 0$, $a = 1.8$, $\lambda = 21.0$, and $\alpha = 1.2$. All values are given in reduced units of $\sigma = 2.0951$ A and $\varepsilon = 2.167$ eV/atom.

In the present simulation, Pd atoms were set in a face-centered-cubic (FCC) lattice within a cubic box. We established a supercell with $14 \times 14 \times 14$ unit cells containing 10 976 atoms, respectively. The Si atoms were set in a supercell of diamond lattice with $14 \times 14 \times 14$ unit cells containing 21 952 atoms. The periodic boundary conditions are applied in all directions. The voids of different sizes are generated by removing atoms inside, as in $1 \times a$ nm, $2 \times a$ nm, $2.5 \times a$ nm, and so on (a denotes the lattice parameter).

After being relaxed near 0 K, these samples underwent a heating process consisting of a series of NPT-MD simulations from 0 to 2600 K with a temperature increment of 200 K. After each stage, we used NVT-MD simulations to balance the heating in the case of the overheating somewhere in the matrix. The desired temperature and ambient pressure were maintained by a Nose–Hoover thermostat and Berendsen method. The equations of atomic motion were integrated by the Verlet velocity algorithm with a time step 1 fs.

3. RESULTS AND DISCUSSION

The transition temperature from the solid to liquid phase is usually identified by studying the variation of thermodynamic properties such as potential energy or some structural properties such as radial distribution function.[32] The phase transition from a solid to a liquid and vice versa can be identified by a simple jump in the volume curve and total potential energy curve. In Figure 1,

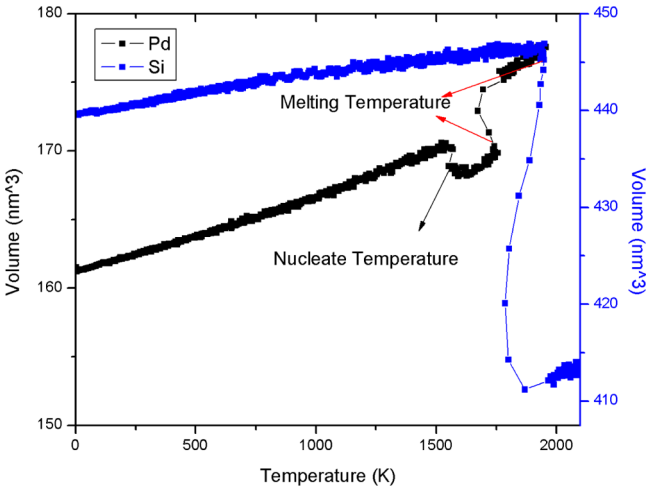

Figure 1. Volume versus temperature of Pd and Si. The void sizes are 0.9725 nm in the Pd matrix (contains 249 Pd atoms) and 1.086 nm in the Si matrix (contains 278 Si atoms).

it can be seen that at 1760 K there is a sudden volume expansion indicating that the whole Pd changes from the solid to liquid. The void melting process of Pd in Figure 2 is similar to the void melting of Ar reported by Li.[4] The melting process of Pd can be divided into four stages. Stage I: ($T < T_n$) (T_n is nucleate temperature), the matrix is stable (Figure 2(a)). Stage II: ($T = T_n$)

DOI: 10.1021/jp5117245
J. Phys. Chem. C 2015, 119, 6843–6851

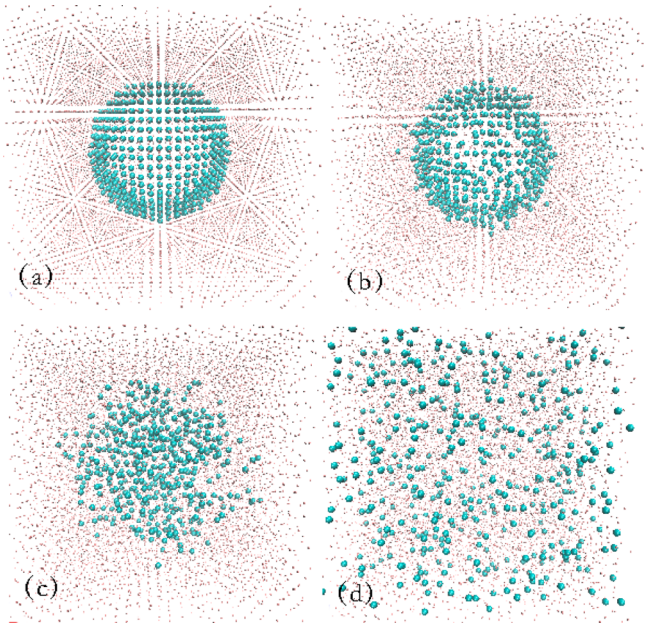

Figure 2. Snapshots of a nanovoid in the Pd matrix during melting (the "bigger" atoms are several layers of atoms around the nanovoid). (a) Initial structure of the nanovoid; (b) starting to nucleate; (c) liquid atoms filling in the nanovoid; (d) the whole matrix melts.

when the temperature reaches T_n, the liquid phase will prefer to nucleate on the inner surface of the nanovoids (Figure 2(b)). Considering the volume−temperature curve in Figure 1, T_n is about 1550 K, and the volume suddenly shrinks from 170.53 to 168.42 nm^3. The volume changes because the atoms move into the void, forming a liquid shell. Stage III: ($T_n < T < T_m$), the partially melted solid fills the void, the liquid and solid coexist, but the matrix is still stable at this temperature (Figure 2(c)). In the volume−temperature curve, the volume increases smoothly again. Stage IV: completely melting (Figure 2(d)), while the whole matrix becomes liquid with the increase of volume.

According to the volume−temperature curve of Si in Figure 1, we can determine the melting point of Si to be 1950 K. It is interesting to point out that the volume of Pd becomes larger at the melting point, while the volume of Si becomes smaller.[33] Obviously, the volume of Pd shrinks suddenly (Figure 1), but there is no shrink phenomenon in the Si during the heating process. Figure 3 shows the gradual change in size and shape of

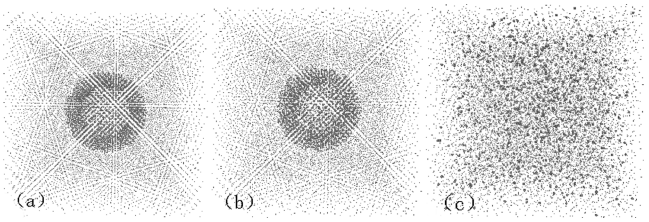

Figure 3. Snapshots of the melting process of a nanovoid in the Si matrix (the "bigger" atoms are several layers of atoms around the nanovoid). (a) Initial structure of the nanovoid; (b) the nanovoid changing without nucleation; (c) the whole matrix melts.

the nanovoid in the Si matrix during the heating at several representative temperatures. Associated with the volume−temperature curve of Si in Figure 1, Figure 3(a,b) shows that the nanovoid keeps a spherical shape all the time with a little volume variation. After the whole matrix melts, the nanovoid disappears and disperses as many small vacancies (Figure 3(c)). This phenomenon has been found in experiments.[22−24]

To analyze the melting mechanism of Pd and Si in detail, we divided the matrix into four layers according to their bond-length (BL) variation region,[34,35] i.e., regions 1, 2, 3, and 4. Figure 4

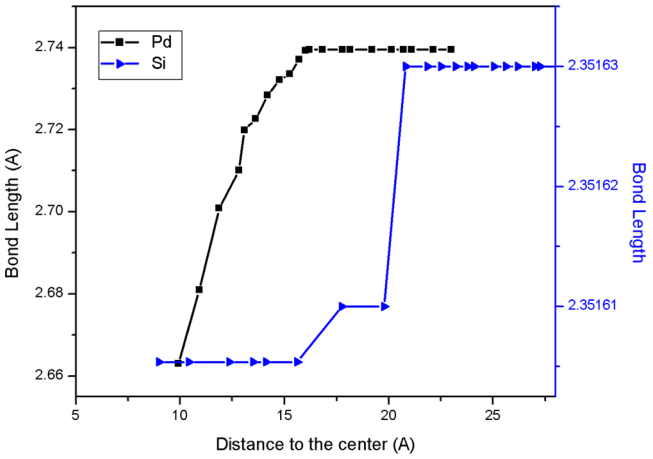

Figure 4. Bond length versus the distance to the center for the matrix in Pd (void size: 0.9725 nm) and Si (void size: 1.086 nm).

shows the BL variation with the distance to void center. It is obvious that the BL of Pd atoms changed from 0.266 to 0.274 nm, and the variation is about 2.91%. However, the BL of Si atoms almost keeps unchanged. From Figure 4, we find that the region of atoms with changed BL is in the inner "surface" layer with thickness of 0.7 nm. Thus, the thickness of the first layer was chosen as about 0.7 nm in Pd and Si. The other regions were divided according to the same thickness. The schematic of the regions is shown in Figure 5.

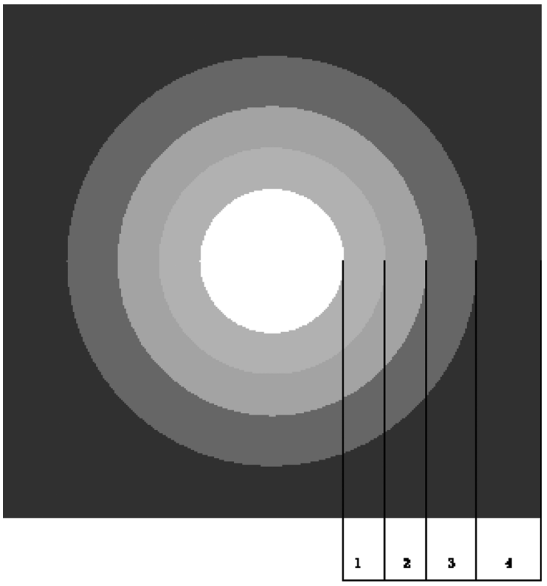

Figure 5. Schematic of four regions from a matrix with a void.

Figure 6(a) shows the average potential energy of each atom at different layers in the Pd matrix. At first, the potential energy of the "surface" atoms (in region 1, these atoms have a lot of dangling bonds) is smaller than those of the "outer" atoms in

DOI: 10.1021/jp5117245
J. Phys. Chem. C 2015, 119, 6843−6851

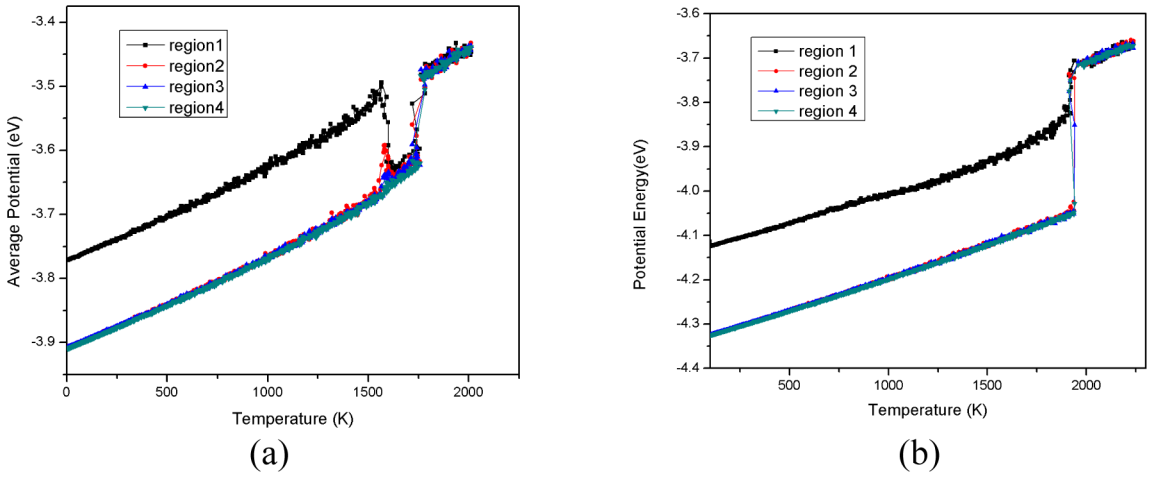

Figure 6. Average atomic potential energy in different shells versus the temperature. (a) Pd; (b) Si.

regions 2, 3, and 4.[36−38] At the nucleate temperature T_n, the surface begins to melt, and the nanovoid starts to shrink. After shrinking, the dangling bonds disappear, and the average atom potential energy comes to equal. At the melting point T_m, the whole solid changes to liquid, and the potential energy increases suddenly correspondingly. Figure 6(b) gives the average potential variation for the Si matrix. The potential energy of atoms in region 1 is smaller than those of the atoms in other regions (2−4) first, which is similar to the case of Pd mentioned above. However, there is no sudden change for the energy of atoms in region 1 before melting, which means there is no apparent nucleate temperature. This phenomenon is different from the case of Pd, indicating that there is no nucleation process for the void melting of Si solids. The average potential energy of all atoms comes to equal after melting, although the energy in region 1 is always higher than that of other regions before melting.

Pair correlation function ($g(r)$) is a function that describes the spherically averaged local organization around any given atom,[39] by which the structure variation can be characterized. Figure 7 presents the computed $g(r)$ of four regions at different temperatures. According to the $g(r)$ of Pd (Figure 7(a)∼(c)), there are sharp peaks at lower temperature (800 K), indicating that the atoms sited at their lattice points. At 1560 K, the second peak in the $g(r)$ curve of region 1 disappears; however, the second peak in other regions still exists, indicating that the atoms in region 1 become disordered first. When the temperature approaches the melting temperature 1760 K, the $g(r)$ curves of all regions become almost the same. The $g(r)$ curves at different temperature of Si are presented in Figure 7(d)∼(f). It is found that the $g(r)$ curves of all four regions are almost the same at the specified temperature. At 600 K, there are sharp peaks in $g(r)$ curves of four regions. At 1870 K, near its melting temperature, the second peak and the third peak come to combine together. At 1960 K, the $g(r)$ shows the character of the liquid, indicating the total matrix melt. For the $g(r)$ variation during melting, the void structure variation of Pd is different from that of Si, indicating that there exist different melting mechanisms for void melting.

4. THERMODYNAMIC CRITERIA FOR TWO MECHANISMS OF VOID MELTING

According to surface melting theory,[25] for a flat surface, the surface melting occurs only if $\Delta\gamma > 0$, while $\Delta\gamma = \gamma_{sv} - (\gamma_{sl} + \gamma_{lv})$ (γ represents interface energy, and subscripts s = solid, l = liquid, and v = vapor). For nanovoids, the interface energy depends on void size (r)[17,18]

$$\frac{\gamma_{sv}(r)}{\gamma_{sv}^0} \approx \frac{\gamma_{lv}(r)}{\gamma_{lv}^0} = \left[1 + \frac{1}{\frac{4r}{h} + 1}\right] \times \exp\left[\frac{2S_b}{3R\left(\frac{4r}{h} + 1\right)}\right] \quad (7)$$

$$\frac{\gamma_{sl}(r)}{\gamma_{sl}^0} = 1 + \frac{3h}{2r} \quad (8)$$

where $S_b = E_b/T_b$, the cohesive entropy of crystals, equals the ratio between the bulk cohesive energy (E_b) and bulk boiling point (T_b). h is the atomic diameter, and R, the gas constant, equals 8.314 J/mol·K. The needed parameters are listed in Table 1.

For Pd, the γ_{sv}, γ_{sl}, and γ_{lv} are 1.808, 0.302, and 1.480 J/m^2,[40] respectively, and thus $\Delta\gamma = 0.026$ J/m^2. For Si, the γ_{sv}, γ_{sl}, and γ_{lv} are 1.038, 0.416, and 0.800 J/m^2,[40] respectively, and thus $\Delta\gamma = -0.178$ J/m^2. When the condition $\Delta\gamma > 0$ cannot be satisfied for Si, there will be no liquid nucleation before melting. For Pd, the condition $\Delta\gamma > 0$ (Figure 8(a,b)) is satisfied well, and the liquid phase will nucleate at the inner surface to form a liquid layer before melting.

As mentioned above, Li et al.[4] have simulated the void melting of Ar using MD simulation, which can be used as an example to test the above criteria for determining the melting mechanism. The $\Delta\gamma > 0$ of Ar equals 0.00282 J/m^2 (see Table 2), larger than zero, and thus its melting should follow the NM mechanism according to the criteria. Fortunately, Li's work just indicated that void melting in Ar is the NM mechanism. We also simulated the void melting in Au, Al, and Co solids; their melting processes are the same as that of Pd, following the NM mechanism. By computing the $\Delta\gamma > 0$ of the three solids, we found that the values are all positive, and their melting mechanisms should follow the NM mechanism, which agree well with our simulation results. The input parameters and computational results are listed in Table 2. The criteria for determining the melting mechanism using $\Delta\gamma > 0$ may be regarded as a universal law for void melting.

Figure 8(c,d) shows that the $\Delta\gamma$ of the nanovoid in Si becomes larger than 0 only when its size decreases to a very small value. Figure 9(a,b) compared the different melting processes of Si. In Figure 9(b), there is a sudden change in the average potential energy curve of region 1 atoms in the Si matrix with a nanovoid whose radius is 0.4073 nm at about 1820 K. This behavior is like

DOI: 10.1021/jp5117245
J. Phys. Chem. C 2015, 119, 6843−6851

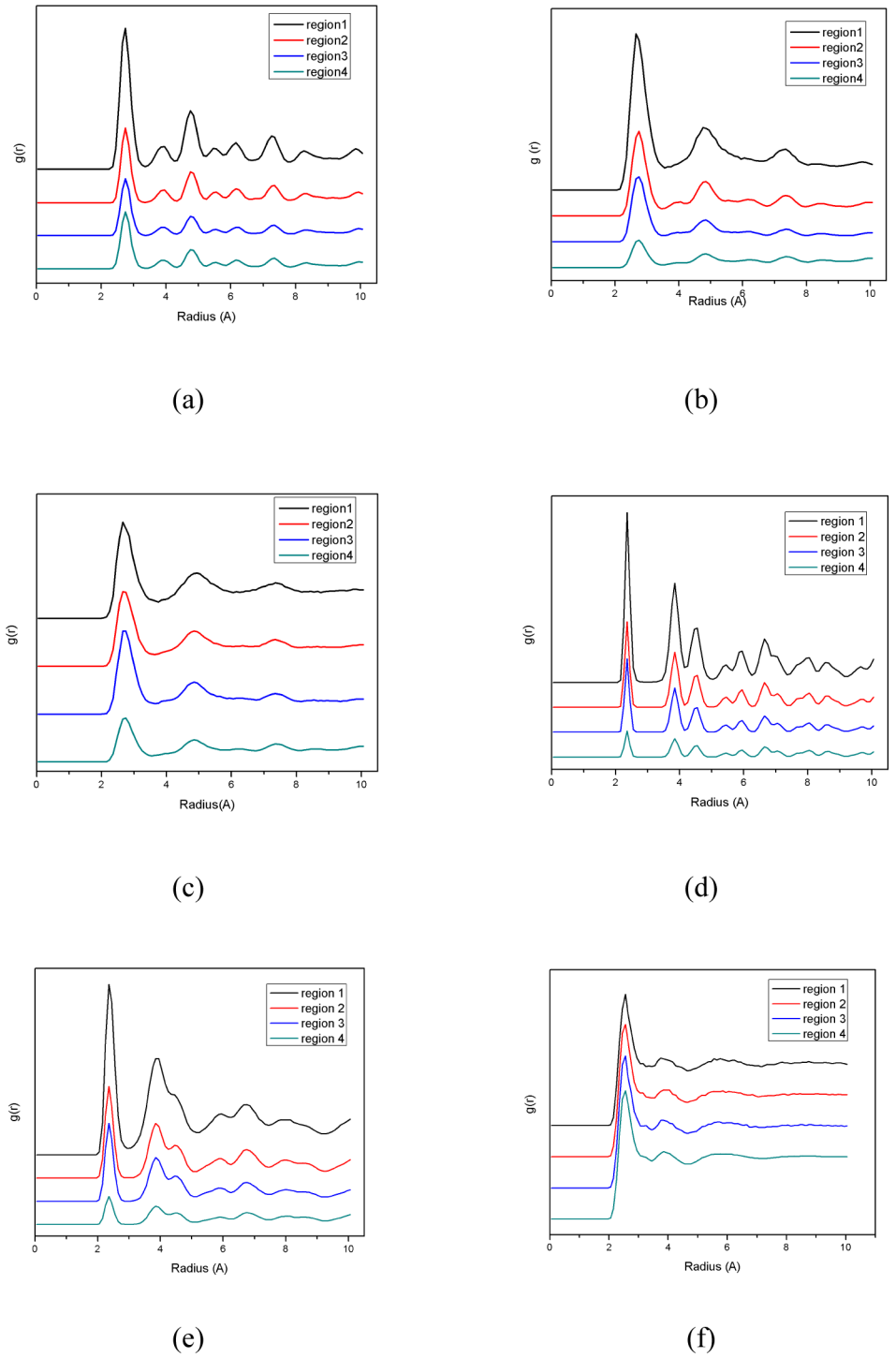

Figure 7. Pair correlation functions of Pd and Si at different temperature. (a) Pd at 800 K; (b) Pd at 1560 K; (c) Pd at 1760 K; (d) Si at 600 K; (e) Si at 1870 K; (f) Si at 1960 K.

Table 1. Input Parameters for Equations 7, 8, 11, and 12

	h (nm)	E_b (kJ/mol)	T_b (K)	S_b (J/(mol·K))	V_{ms} (cm^{-3}/mol)	V_{ml} (cm^{-3}/mol)	H_m^0 (kJ/mol)	B (GPa)
Si	0.157[16]	384.2[16]	3540[16]	108.5[16]	12.02[40]	10.895[40]	50.21[40]	181[40]
Pd	0.274[40]	376[40]	3236[40]	116.2[40]	8.85[40]	10.25[40]	16.7[40]	121[40]

the average potential energy change of Pd with a nanovoid of 0.9725 and 0.389 nm in Figure 9(d). However, we could not observe a significant shrink phenomenon in the volume/temperature curve of a 0.389 nm nanovoid (Figure 9(c)) like the volume/temperature curve change of a 0.9725 nm nanovoid in Pd. However, the average potential energy can tell the change clearly (Figure 9(d)). The reason is the nucleate region's size. According to our research, if the radius of a nanovoid decreases to a small

DOI: 10.1021/jp5117245
J. Phys. Chem. C 2015, 119, 6843−6851

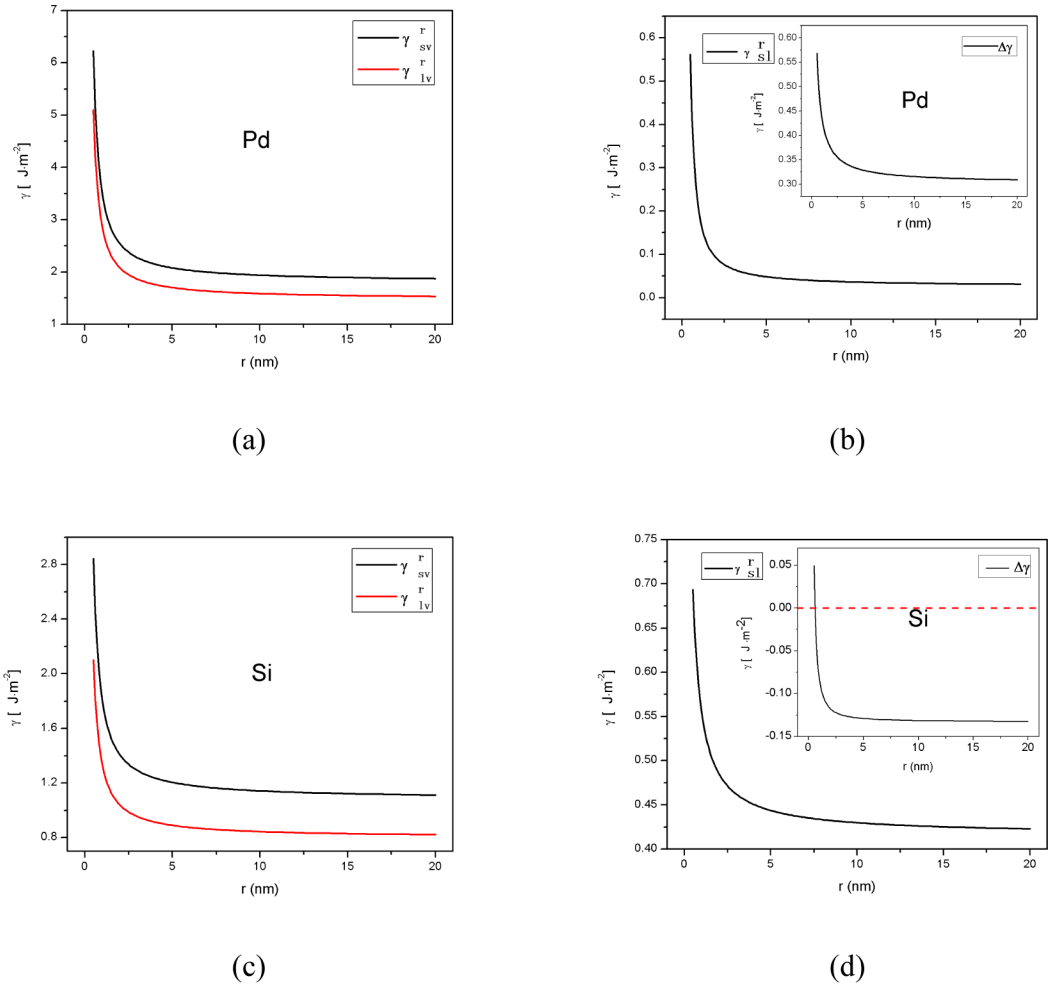

Figure 8. Size-dependent interface energy of voids caluculated by eqs 7 and 8. (a) $\gamma_{sv}(r)$ and $\gamma_{lv}(r)$ of Pd; (b) $\gamma_{sl}(r)$ and $\Delta\gamma(r)$ of Pd; (c) $\gamma_{sv}(r)$ and $\gamma_{lv}(r)$ of Si; and (d) $\gamma_{sl}(r)$ and $\Delta\gamma(r)$ of Si.

Table 2. Thermodynamic Quantities Related to Surface Melting for a Number of Common Elements

	T_m (K)[41]	γ_{sv} (J/m^2)[42]	γ_{sl} (J/m^2)[42]	γ_{lv} (J/m^2)[42]	$\Delta\gamma$ (J/m^2)
Pd	1828	1.808	0.302	1.480	0.026
Si	1683	1.038	0.416	0.800	−0.178
Au	1336	1.362	0.200	1.130	0.033
Co	1766	2.197	0.345	1.830	0.022
Al	931.7	1.032	0.154	0.865	0.013
Ar	83.81[a]	0.0188[a]	0.00428[a]	0.0117[a]	0.00282

[a]The values are from reference 4.

value, when the nucleate condition could be satisfied (the NM mechanism is dominant at that size), the nucleated liquid atoms will overcome the volume Gibbs free energy change, the interface free energy, and the elastic energy change deduced by interface stress.[17] In the following, we will use a model to explain this in detail.

At the nucleate temperature T_n, the matrix with the nanovoid will melt from the inner surfaces, which leads to the formation of a liquid layer. According to Li's model,[17] liquid will nucleate on the surface of the void. As shown in Figure 10, for a void with radius r, the liquid layer results in a solid−liquid interface (curvature radius is r_c) and a liquid−vapor interface (curvature radius is r_l). Then the Gibbs free energy ΔG is[17]

$$\Delta G = \Delta G_v + \Delta G_s + \Delta G_e \quad (9)$$

where ΔG_v, ΔG_s, and ΔG_e are the Gibbs free energy variations induced from volume change, interface, and interface stress, respectively.

$$\Delta G_v = \frac{\frac{4}{3}\pi(r_c^3 - r^3)g_m(T)}{V_{ms}}$$

$$\Delta G_s = \Delta\gamma(\gamma_{lv}^0\gamma_l^2 + \gamma_{sl}^0\gamma_c^2 - \gamma_{sv}^0\gamma^2)$$

$$\Delta G_e = \left(-\frac{2\gamma_{lv}^0}{\gamma_l}\right)V_l + \left[\left(-\frac{2\gamma_{lv}^0}{\gamma_l}\right) + \left(-\frac{2f_{sl}}{r_c}\right)\right]V_c - \left(-\frac{2f_{sv}}{r}\right)V_s$$

V_{ms} and V_{ml} are the solid molar volume and liquid molar volume, respectively.

Assuming that the fluid has little effect on the surface strain of solids, we have the surface stress $f = f_{sl} \approx f_{sv}$, and f has the form[43]

$$f = [(3h\gamma_{sl}^0)B/4]^{1/2} \quad (10)$$

B is the volume elastic modulus.

$$V_c = V_s - \frac{4\pi(r_c^3 - r^3)}{3}$$

$$V_l = \frac{4\pi(r_c^3 - r^3)V_{ml}}{3V_{ms}}$$

DOI: 10.1021/jp5117245
J. Phys. Chem. C 2015, 119, 6843−6851

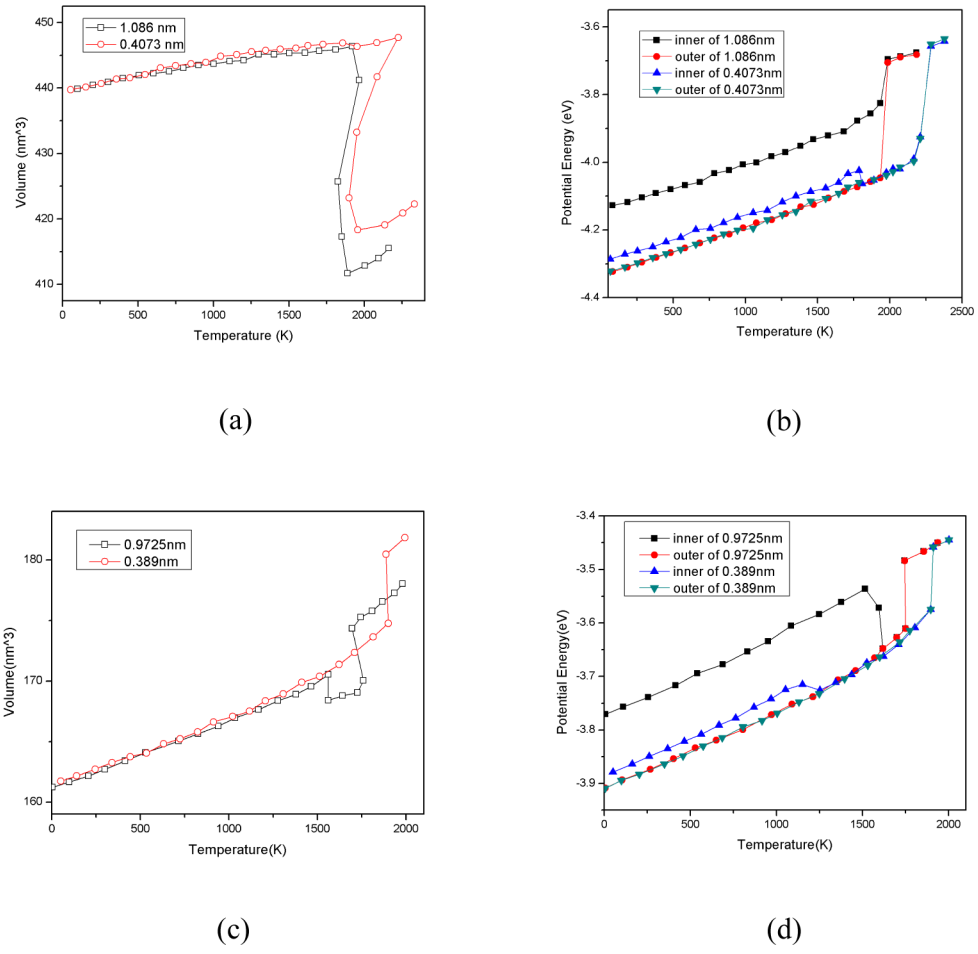

Figure 9. (a) Volume versus temperature of Si solids with voids of 0.1.086 and 0.4073 nm; (b) average potential energy of "inner" and "outer" regions of the solids (the inner region is the region 1 in Figure 5, and the outer regions are regions 2–4 in Figure 5); (c) volume versus temperature of Pd solids with voids of 0.9725 and 0.389 nm; (d) average potential energy of "inner" and "outer" regions of the solids.

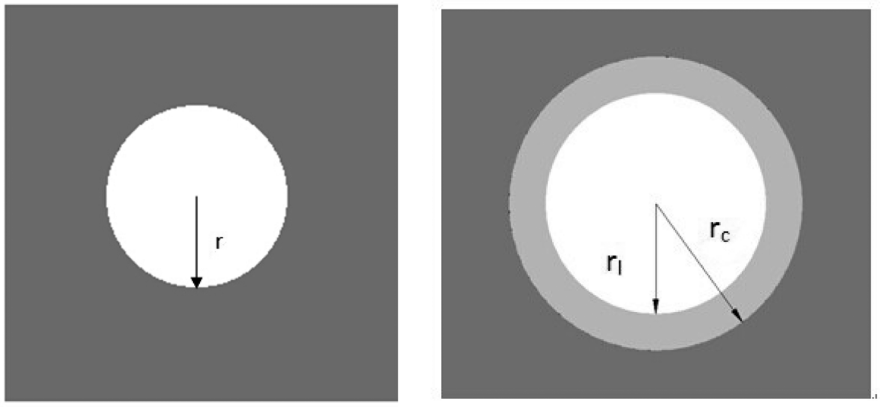

Figure 10. Schematic of surface melting of a nanovoid.

$$g_m(T) = H_m^0 - TS_m^0 \approx H_m^0(1 - T/T_m^0) \quad (11)$$

H_m^0 and S_m^0 are the bulk melting enthalpy and entropy, respectively.

Let $\partial\Delta G(r,T,r_c)/(\partial r_c) = 0$, we have

$$g_m(T) + \frac{2\gamma_{lv}^0(V_{ms} - V_{ml})}{r} + \frac{2V_{ms}(\gamma_{sl}^0 + f)}{r_c^*} - \frac{2fV_{ms}\left[1 - \left(\frac{r}{r_c^*}\right)^3\right]}{3r_c^*} = 0 \quad (12)$$

Using eqs 11 and 12, we can obtain $r_c^* = 3.705$ nm for voids in the Pd matrix at 1550 K when $r = 0.9725$ nm, and $r_c^* = 0.62$ nm for voids in the Pd matrix at about 1150 K when $r = 0.389$ nm (the needed parameters are listed in Table 1 and Table 2).

We also studied the melting temperature of solids with voids of different sizes. According to our simulation, the melting temperature decreases with the increase of void size, and reaches a plateau at a critical value, which has been explored theoretically in the literature.[4] In the Pd solid matrix of size 14 × 14 × 14 units,

DOI: 10.1021/jp5117245
J. Phys. Chem. C 2015, 119, 6843–6851

the simulated melting temperature is 1885 K, but when the void's radius is 2.5 × 0.389 nm, the matrix melting temperature becomes 1760 K, lower than 1885 K. When the nanovoid's radius is 1 × 0.389 nm, the matrix melting temperature is 1890 K. The simulated melting temperature of the 14 × 14 × 14 units Si solid matrix is about 2090 K, and when the void radius is 1.086 nm, the melting temperature is 1950 K; however the Si solid may be local superheated (the melting temperature is higher than 2090 K) when it consists of a void with size smaller than 0.4073 nm (radius). It is concluded that in the two melting mechanism, the existence of a large void in the solid could reduce the local melting temperature of the matrix. However, void melting may lead to the superheating of the matrix when the void size is smaller than a critical value.

5. CONCLUSIONS

In this work, we have studied the melting of nanovoids by using the MD simulation and found that there exist two different melting mechanisms for void melting: the NM and the NNM mechanisms. The void melting of a solid follows the NM or NNM mechanism due to the positive or negative values of $\Delta\gamma(r)$. If $\Delta\gamma(r) < 0$, the void melting follows the NNM mechanism, and the void will start with a gradual shrink to a critical value during heating and disappears with the whole matrix melting. However, if $\Delta\gamma(r) > 0$, the void melting follows the NM mechanism, while the surface of the void starts to melt first and the liquid nucleates on the inner surface. The present simulation and findings unify the two different melting mechanisms and present a clear picture for void melting.

AUTHOR INFORMATION

Corresponding Author

*E-mail: qiwh216@csu.edu.cn (W. H. Qi).

Notes

The authors declare no competing financial interest.

ACKNOWLEDGMENTS

This work was supported by National Nature Science Foundation of China (Grant No. 21373273), Hunan Provincial Natural Science Foundation of China (Grant No. 13JJ1002), and Shenghua Scholar Program of Central South University. The simulation was carried out on the supercomputer of High Performance Computing Center at Central South University.

REFERENCES

(1) Zhu, X. Shrinkage of nanocavities in silicon during electron beam irradiation. *J. Appl. Phys.* **2006**, *100*, 034304.
(2) Li, S. Q.; Qi, W. H. Calculation of absorption spectrum of silver-gold bimetallic nanoparticles. *Acta Phys. Sin.* **2014**, *63*, 117802.
(3) Agrawal, P. M.; Raff, L. M.; Komanduri, R. Monte Carlo simulations of void-nucleated melting of silicon via modification in the Tersoff potential parameters. *Phys. Rev. B* **2005**, *72*, 125206.
(4) Bai, X. M.; Li, M. Nucleation and melting from nanovoids. *Nano Lett.* **2006**, *6* (10), 2284−2289.
(5) Agrawal, P. M.; Rice, B. M.; Thompson, D. L. Molecular dynamics study of the effects of voids and pressure in defect-nucleated melting simulations. *J. Chem. Phys.* **2003**, *118*, 9680−9688.
(6) Bachels, T.; Güntherodt, H. J.; Schäfer, R. Melting of isolated tin nanoparticles. *Phys. Rev. Lett.* **2000**, *85*, 1250−1253.
(7) Velardez, G. F.; Alavi, S.; Thompson, D. L. Molecular dynamics studies of melting and solid-state transitions of ammonium nitrate. *J. Appl. Phys.* **2004**, *120*, 9151−9159.
(8) Li, S. Q.; Qi, W. H.; Peng, H. C.; Wu, J. Z. A Comparative Study on Melting of Core-shell and Janus Cu-Ag Bimetallic Nanoparticles. *Comput. Mater. Sci.* **2015**, *99*, 125−132.
(9) Qi, W. H.; Wang, M. P. Size and shape dependent melting temperature of metallic nanoparticles. *Mater. Chem. Phys.* **2004**, *88*, 280−284.
(10) Jiang, H.; Moon, K.; Dong, H.; et al. Size-dependent melting properties of tin nanoparticles. *Chem. Phys. Lett.* **2006**, *429*, 492−496.
(11) Alavi, S.; Thompson, D. L. Molecular dynamics simulations of the melting of aluminum nanoparticles. *J. Phys. Chem. A* **2006**, *110*, 1518−1523.
(12) Sheng, H. W. Superheating and melting-point depression of Pb nanoparticles embedded in Al matrices. *Philos. Mag. Lett.* **1996**, *73*, 179−186.
(13) Qi, W. H.; Wang, M. P. Size-and shape-dependent superheating of nanoparticles embedded in a matrix. *Mater. Lett.* **2005**, *59*, 2262−2266.
(14) Zhong, J.; Zhang, L. H.; Jin, Z. H.; et al. Superheating of Ag nanoparticles embedded in Ni matrix. *Acta Mater.* **2001**, *49*, 2897−2904.
(15) He, A. M.; Duan, S.; Shao, J. L. Shock melting of single crystal copper with a nanovoid: Molecular dynamics simulations. *J. Appl. Phys.* **2012**, *112*, 074116.
(16) Lu, H. M.; Ding, D. N.; Cao, Z. H. Surface energy and melting temperature of elemental nanocavities. *J. Phys. Chem. C* **2007**, *111*, 12914−12917.
(17) Li, H.; Wen, Z.; Jiang, Q. Liquid nucleation of surface-free crystal from nanovoids. *Solid State Commun.* **2008**, *147*, 250−253.
(18) Ouyang, G.; Wang, C. X.; Yang, G. W. Surface energy of nanostructural materials with negative curvature and related size effects. *Chem. Rev.* **2009**, *109*, 4221−4247.
(19) Ouyang, G.; Tan, X.; Cai, M. Q. Surface energy and shrinkage of a nanocavity. *Appl. Phys. Lett.* **2006**, *89*, 183104.
(20) Ouyang, G.; Li, X. L.; Yang, G. W. Superheating and melting of nanocavities[J]. *Appl. Phys. Lett.* **2008**, *92*, 051902.
(21) Zhu, X. F.; Williams, J. S.; Conway, M. J. Direct observation of irradiation-induced nanocavity shrinkage in Si. *Appl. Phys. Lett.* **2001**, *79*, 3416−3418.
(22) Williams, J. S.; Zhu, X.; Ridgway, M. C. Preferential amorphization and defect annihilation at nanocavities in silicon during ion irradiation. *Appl. Phys. Lett.* **2000**, *77*, 4280−4282.
(23) Ruault, M. O.; Fortuna, F.; Bernas, H. In situ transmission electron microscopy ion irradiation studies at Orsay. *J. Mater. Res.* **2005**, *20*, 1758−1768.
(24) Zhu, X. F. Nanocavity shrinkage and preferential amorphization during irradiation in silicon. *Chin. Phys. Lett.* **2005**, *22*, 657−660.
(25) Kofman, R.; Cheyssac, P.; Aouaj, A.; et al. Surface melting enhanced by curvature effects. *Surf. Sci.* **1994**, *303*, 231−246.
(26) Plimpton, S. Fast Parallel Algorithms for Short-Range Molecular Dynamics. *J. Comp. Phys.* **1995**, *117*, 1−19.
(27) Foiles, S. M.; Baskes, M. I.; Daw, M. S. Embedded-atom-method functions for the fcc metals Cu, Ag, Au, Ni, Pd, Pt, and their alloys. *Phys. Rev. B* **1986**, *33*, 7983−7991.
(28) Daw, M. S.; Foiles, S. M.; Baskes, M. I. The embedded-atom method: a review of theory and applications. *Mater. Sci. R.* **1993**, *9*, 251−310.
(29) Stillinger, F. H.; Weber, T. A. Computer simulation of local order in condensed phases of silicon. *Phys. Rev. B* **1985**, *31*, 5262−5271.
(30) Blaisten-Barojas, E.; Levesque, D. Molecular-dynamics simulation of silicon clusters. *Phys. Rev. B* **1986**, *34*, 3910−3916.
(31) Thijsse, B. J. Relationship between the modified embedded-atom method and Stillinger-Weber potentials in calculating the structure of silicon. *Phys. Rev. B* **2002**, *65*, 195207.
(32) Sankaranarayanan, S. K. R. S.; Bhethanabotla, V. R.; Joseph, B. Molecular dynamics simulation study of the melting of Pd-Pt nanoclusters. *Phys. Rev. B* **2005**, *71*, 195415.
(33) Zhang, Q.; Li, Q.; Li, M. Melting and superheating in solids with volume shrinkage at melting: A molecular dynamics study of silicon. *J. Chem. Phys.* **2013**, *138*, 044504.
(34) Qi, W. H.; Huang, B. Y.; Wang, M. P. Structure of unsupported small palladium nanoparticles. *Nanoscale Res. Lett.* **2009**, *4*, 269−273.

DOI: 10.1021/jp5117245
J. Phys. Chem. C 2015, 119, 6843−6851

(35) Qi, W. H.; Huang, B. Y.; Wang, M. P. Bond-length and-energy variation of small gold nanoparticles. *J. Comput. Theor. Nanosci.* **2009**, *6*, 635−639.
(36) Pauling, L. Atomic radii and interatomic distances in metals. *J. Am. Chem. Soc.* **1947**, *69*, 542−543.
(37) Goldschmidt, V. M. Crystal structure and chemical correlation. *Ber. Deut. Chem. Ges.* **1927**, *60*, 1270.
(38) Sun, C. Q. Size dependence of nanostructures: Impact of bond order deficiency. *Prog. Solid State Chem.* **2007**, *35*, 1−159.
(39) Kart, H. H.; Yildirim, H.; Ozdemir, K. S.; Çagin, T. Physical properties of Cu nanoparticles: A molecular dynamics study. *Mater. Chem. Phys.* **2014**, *15*, 204−212.
(40) Wikipedia; http://en.wikipedia.org/wiki/Chemical_element
(41) Kittel, C. *Introduction to solid state physics*; Wiley: New York, 1996.
(42) Vanselow, R.; Howe, R. *Chemistry and physics of solid surfaces VII*; Springer press: Germany, 1988.
(43) Jiang, Q.; Liang, L. H.; Zhao, D. S. Lattice contraction and surface stress of fcc nanocrystals. *J. Phys. Chem. B* **2001**, *105* (27), 6275−6277.

DOI: 10.1021/jp5117245
J. Phys. Chem. C 2015, 119, 6843−6851